Improved technique for measuring full-field absolute phases in a common-path heterodyne interferometer

Yen-Liang Chen and Der-Chin Su*

Department of Photonics and Institute of Electro-Optical Engineering, National Chiao-Tung University, 1001 Ta-Hsueh Road, Hsinchu 30010, Taiwan

*Corresponding author: t7503@faculty.nctu.edu.tw

Received 3 May 2010; accepted 2 August 2010;
posted 5 August 2010 (Doc. ID 127814); published 30 August 2010

When an asymmetric triangle voltage signal is applied to drive an electro-optic modulator, interference signals with two groups of periodic sinusoidal segments with different frequencies are obtained. An improved method is proposed to fit these two groups of segments, and their associated phases can be determined. The absolute phase can be obtained by subtracting the initial phase from the phases of these two groups. This technique is applied to all pixels, and the full-field absolute phase measurements can be achieved. The validity of this method is demonstrated. © 2010 Optical Society of America

OCIS codes: 230.2090, 040.2840, 120.5050, 120.3180.

1. Introduction

In our previous paper [1], a method was proposed for determining full-field absolute phases in heterodyne interferometry [2–10]. In that method, the sawtooth voltage signal with the amplitude being lower than its half-wave voltage is used to drive the electro-optic modulator. A group of periodic sinusoidal segments at every pixel is obtained. The period of the sampled sinusoidal segments is lengthened, and they are modified to an associated continuous sinusoidal wave, and the absolute phase can be determined. However, a characteristic phase exists to be subtracted, and its error contributes the total measurement error. In addition, enough sample periods should be taken for an iteration process to find the optimum segment [1] and decrease the phase error. Consequently, the entire process is certainly complex in the previous method. To overcome these drawbacks, an improved technique for measuring the full-field absolute phases is proposed in this paper. The electro-optic modulator is driven with an asymmetric triangle voltage signal instead of the conventional sawtooth voltage signal, and the interference signals with two groups of periodic sinusoidal segments with different frequencies at every pixel are obtained. The phase difference of these two sinusoidal segments depends only on the absolute phase and is not related to the initial phase of a certain sampled starting point in the time axis. In real measurements, these sinusoidal segments are taken by a fast camera and become discrete digital signals. After the second order differential operations, the sinusoidal segments are divided into two groups, according to their frequencies. Next, a modified least-squares sine fitting algorithm is used to calculate the phases of these two groups, and the absolute phase measured at the pixel can be derived. These operations are applied to other pixels, and full-field absolute phase measurements can be achieved. The validity of this method is demonstrated. It has merits of both easy operation and high accuracy, compared to the previous method.

2. Principle

A. Waveforms of the Interference Signals

The optical configuration is shown in Fig. 1. Its heterodyne light source consists of a linearly polarized laser source (LS), an electro-optic modulator (EO) with half-wave voltage V_π, a linear voltage amplifier

0003-6935/10/254746-05$15.00/0
© 2010 Optical Society of America

(LVA), and a function generator (FG). For convenience, the $+z$ axis is chosen along the propagation direction, and the y axis is along the vertical direction. A linear polarized light at 45° with respect to the x axis passes through the EO with the axis at 0° with respect to the x axis. If an external voltage V_z is applied to the EO, then the phase retardation between s and p polarizations can be given as [1]

$$\Gamma = \frac{\pi}{V_\pi} V_z. \tag{1}$$

Instead of the conventional sawtooth voltage signal, an asymmetric triangle voltage signal with a period T and an amplitude V_π is used to drive the EO. Its shape is shown as in Fig. 2(a), with a $2/3T$ upward part and a $1/3T$ downward part. They can be expressed as

$$V_Z = \frac{3V_\pi}{T}[(t-t_0) - mT] - V_\pi, \qquad mT \le t - t_0 \le (m + 2/3)T; \tag{2a}$$

$$V_Z = -\frac{6V_\pi}{T}[(t-t_0) - (m+1)T] - V_\pi, \qquad (m + 2/3)T \le t - t_0 \le (m+1)T, \tag{2b}$$

respectively, where m is a nonnegative integer. Substitute Eqs. (2a) and (2b) into Eq. (1), and we have

$$\Gamma = 3\pi\frac{t-t_0}{T} - (m+1)\pi, \qquad mT \le t - t_0 \le (m + 2/3)T; \tag{3a}$$

$$\Gamma = -6\pi\frac{t-t_0}{T} - \pi, \qquad (m + 2/3)T \le t - t_0 \le (m+1)T. \tag{3b}$$

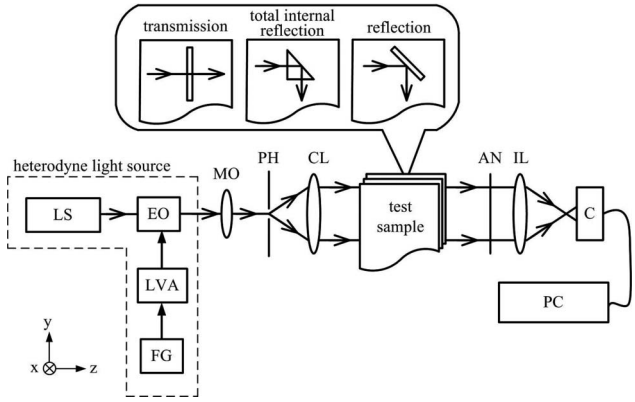

Fig. 1. Schematic diagram for the full-field common-path heterodyne interferometer: LS, linearly polarized laser source; EO, electro-optic modulator; FG, function generator; LVA, linear voltage amplifier; MO, microscopic objective; PH, pinhole; CL, collimating lens; AN, analyzer; IL, imaging lens; C, CMOS camera; PC, personal computer.

In a real measurement, there is an additional phase difference ϕ between s and p polarizations after the light beam passes through (or is reflected by) the test sample, as shown in Fig. 1. Then, it passes through an analyzer (AN) with the transmission axis at 45° with respect to the x axis. Finally, it is imaged on a complementary metal oxide semiconductor (CMOS) camera C by an imaging lens (IL). Hence, the test signal can be written as

$$I(t) = \frac{1}{2}\left[1 + \cos\left(3\pi\frac{t}{T} - \phi_0 + \phi - m\pi\right)\right], \qquad mT \le t - t_0 \le (m + 2/3)T; \tag{4a}$$

$$I(t) = \frac{1}{2}\left[1 + \cos\left(6\pi\frac{t}{T} - 2\phi_0 - \phi\right)\right], \qquad (m + 2/3)T \le t - t_0 \le (m+1)T, \tag{4b}$$

where $\phi_0 = 3\pi t_0/T$ represents the initial phase at the first sampling point, while $t = 0$. For clarity, the interference signals for several different ϕ can be depicted in Figs. 2(b)–2(j). It is obvious that the shape of $I(t)$ is changed with ϕ instead of ϕ_0. If $\psi_1 = -\phi_0 + \phi - m\pi$ and $\psi_2 = -2\phi_0 - \phi$ are measured, then

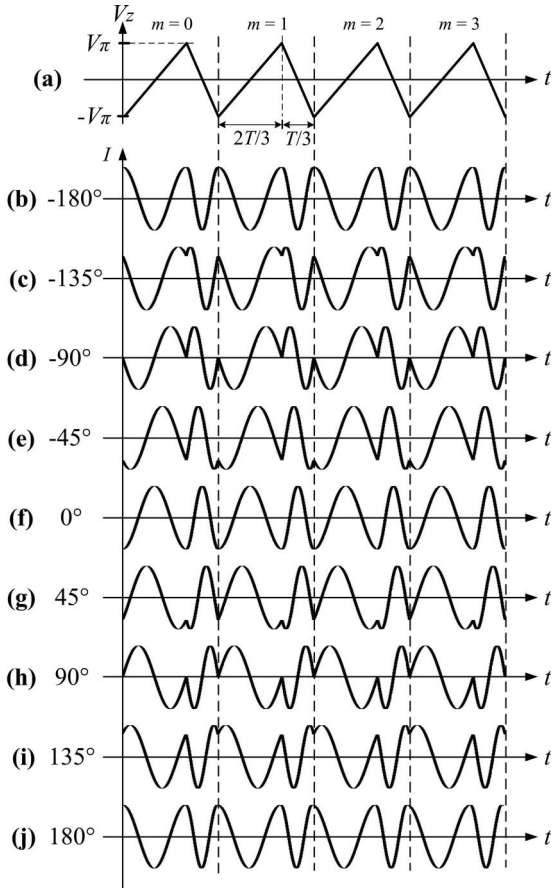

Fig. 2. (a) Asymmetric triangle voltage signal is used to drive the EO. (b)–(j) Theoretical interference signals as ϕ is changed from −180° to 180° in steps of 45°.

the test phase ϕ can be derived from Eqs. (4a) and (4b) and written as

$$\phi = \frac{(2\psi_1 - \psi_2)}{3}. \tag{5}$$

B. Algorithm for Determining Absolute Phases

If the camera C with the frame frequency f_c is used to record n frames at time $0, \Delta t, 2\Delta t, \ldots, (n-1)\Delta t$, where $\Delta t = 1/f_c$, then each pixel records a series of discrete digital signals $I_0, I_1, I_2, \ldots I_{n-1}$, as shown in Fig. 3. The symbols * or ○ mean the sampling positions of the signals of group A and group B, which correspond to Eqs. (4a) and (4b); their frequencies are $f_A = 3/2T$ and $f_B = 3/T$, as shown in Figs. 4(a) and 4(d), respectively. The junctions at any two consecutive sampled sinusoidal segments in the time axis are at local extreme positions, which can be determined by operating the second order differential on the discrete signals. Because there is a π phase difference between the even and the odd segments in group A, Eq. (4a) can be rewritten as

$$I_A(t) = \frac{1}{2}\left[1 + \cos\left(3\pi\frac{t}{T} + \psi_1\right)\right] = A_1 \cdot \cos\left(3\pi\frac{t}{T}\right) + B_1 \cdot \sin\left(3\pi\frac{t}{T}\right) + C_1, \quad \text{if } m \text{ is even;} \tag{6a}$$

$$I_A(t) = \frac{1}{2}\left[1 + \cos\left(3\pi\frac{t}{T} + \psi_1 + \pi\right)\right] = A_1 \cdot -\cos\left(3\pi\frac{t}{T}\right) + B_1 \cdot -\sin\left(3\pi\frac{t}{T}\right) + C_1, \quad \text{if } m \text{ is odd.} \tag{6b}$$

If the data of the odd segments is shifted a π phase, then the signal of group A becomes as that shown in Fig. 4(b) and can be fitted to obtain a continuous sinusoidal wave, as shown in Fig. 4(c). Consequently, Eqs. (6a) and (6b) can further be written as

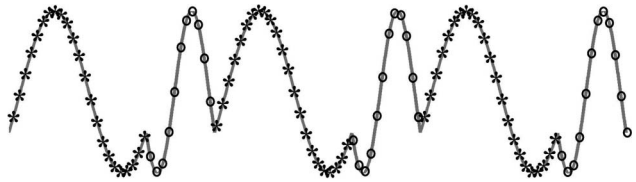

Fig. 3. Sampled data divided into two groups: group A (symbol *) with $f = 3/2T$ and group B (symbol ○) with $f = 3/T$.

where A_1, B_1, and C_1 are real numbers. They can be derived with the least-squares sine fitting algorithm [11], that is,

$$\begin{pmatrix} A_1 \\ B_1 \\ C_1 \end{pmatrix} = (M_1^t M_1)^{-1} M_1^t I_A, \tag{8}$$

where M_1^t means the transpose matrix of M_1. On the other hand, all the segments in group B are in-phase, so they can be fitted directly to obtain a continuous sinusoidal wave, as shown in Fig. 4(e). Equation (4b) can be expressed as

$$I_B(t) = \frac{1}{2}\left[1 + \cos\left(6\pi\frac{t}{T} + \psi_2\right)\right] = A_2 \cdot \cos\left(6\pi\frac{t}{T}\right) + B_2 \cdot \sin\left(6\pi\frac{t}{T}\right) + C_2, \tag{9}$$

where A_2, B_2, and C_2 are real numbers and can be derived similarly by using Eq. (8). Finally, ψ_1 and ψ_2 can be derived and written as

$$\psi_1 = \tan^{-1}\left(\frac{-B_1}{A_1}\right), \tag{10a}$$

$$\psi_2 = \tan^{-1}\left(\frac{-B_2}{A_2}\right). \tag{10b}$$

$$I_A(t) = \begin{pmatrix} I_A(m=0, t=0) \\ I_A(m=0, t=\Delta t) \\ \vdots \\ I_A(1, k\Delta t) \\ I_A(1, (k+1)\Delta t) \\ \vdots \\ I_A(2, (k+Tf_c)\Delta t) \\ \vdots \end{pmatrix} = \begin{pmatrix} \cos\left(3\pi\frac{0}{T}\right) & \sin\left(3\pi\frac{0}{T}\right) & 1 \\ \cos\left(3\pi\frac{\Delta t}{T}\right) & \sin\left(3\pi\frac{\Delta t}{T}\right) & 1 \\ \vdots & \vdots & \vdots \\ -\cos\left(3\pi\frac{k\Delta t}{T}\right) & -\sin\left(3\pi\frac{k\Delta t}{T}\right) & 1 \\ -\cos\left(3\pi\frac{(k+1)\Delta t}{T}\right) & -\sin\left(3\pi\frac{(k+1)\Delta t}{T}\right) & 1 \\ \vdots & \vdots & \vdots \\ \cos\left(3\pi\frac{(k+Tf_c)\Delta t}{T}\right) & \sin\left(3\pi\frac{(k+Tf_c)\Delta t}{T}\right) & 1 \\ \vdots & \vdots & \vdots \end{pmatrix} \times \begin{pmatrix} A_1 \\ B_1 \\ C_1 \end{pmatrix} = M_1 \times \begin{pmatrix} A_1 \\ B_1 \\ C_1 \end{pmatrix}, \tag{7}$$

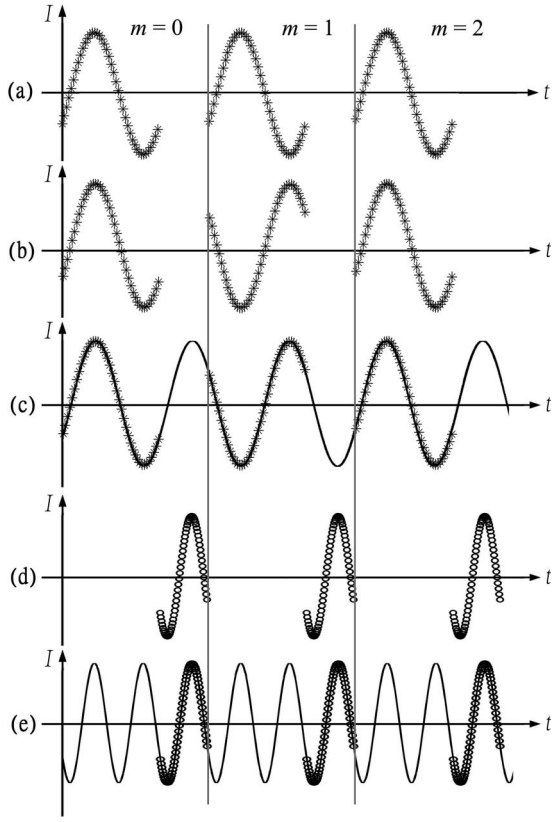

Fig. 4. Processes to obtain associated sinusoidal signals: (a) the sampled data of group A; (b) the odd segments in (a) are shifted a π phase; (c) the associated sinusoidal signals (solid line) of (b); (d) the sampled data of group B; (e) the associated sinusoidal signals (solid line) of (d).

By substituting the results of Eqs. (10a) and (10b) into Eq. (5), the absolute phase ϕ can be calculated. These operations are applied to other pixels, and full-field absolute phase measurements can be achieved. For easy understanding, a flow chart that describes the whole process is summarized and shown in Fig. 5.

3. Experiments and Results

To show the feasibility of this technique, the full-field absolute phase retardations of a quarter-wave-plate were measured. A He–Ne laser with a 632.8 nm wavelength, an EO modulator (New Focus/Model 4002) with $V_\pi = 148$ V, and a CMOS camera (Basler/A504K) with an 8 bit gray level and 200×200 pixels were used. Under the conditions $T = 1$ s and sampling frequency $f_c = 49.1$ frames/s, 500 frames were taken. The intensities of the sampled signals at the pixel $(+100, +100)$ are shown in Fig. 6. The full-field phase retardation measurement is depicted in Fig. 7, where the average phase retardation of the full-field distribution and its standard deviation are 89.9° and 0.5°, respectively.

4. Discussion

In our previous method [1], an iteration process is used to find the optimum segment. The sampled segments can be modified to a continuously sinusoidal wave that can be expressed as

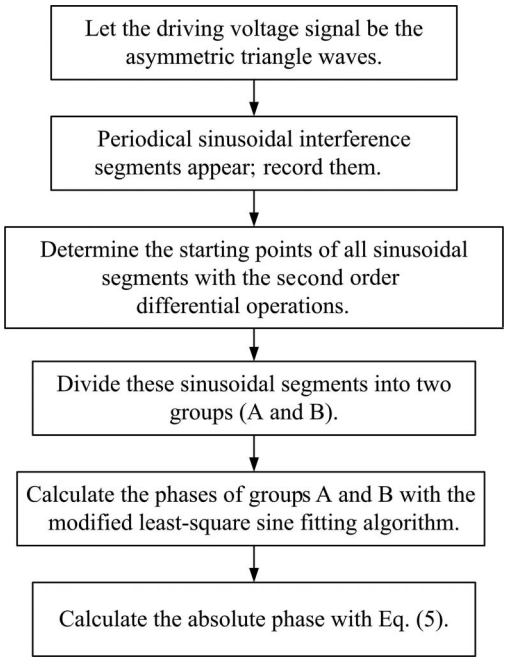

Fig. 5. Flow chart for the whole process.

$$I_c = \frac{1}{2}\left[1 + \cos\left(2\pi \frac{V}{V_\pi T} t + \psi\right)\right], \tag{11}$$

where V is the amplitude of the external sawtooth voltage signal to the EO. The absolute phase can be obtained from the initial phase of the optimum segment. Although the error of determining the starting point of the optimum segment can be decreased by using enough sampled segments under specific experimental conditions, it is difficult to approach the theoretical starting point when f_c is near $nV/V_\pi T$ (n is an integer). The maximum phase error might even reach to $\Delta\psi = 2\pi V/V_\pi T f_c$. However, in this improved technique, groups A and B have the same initial phase. The absolute phase can be derived with subtractive operation without the prior information of the phase at the starting point of each segment. Only several sampled segments are required to determine the absolute phase. Besides, the time axis of the sampled data in this technique

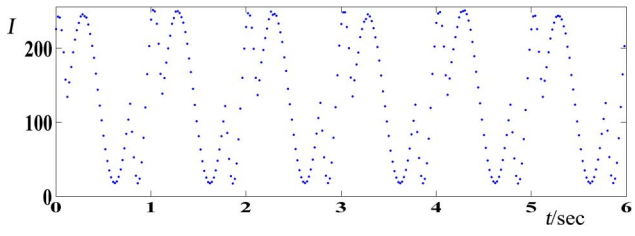

Fig. 6. (Color online) Intensities of the sampled signals at the pixel $(+100, +100)$.

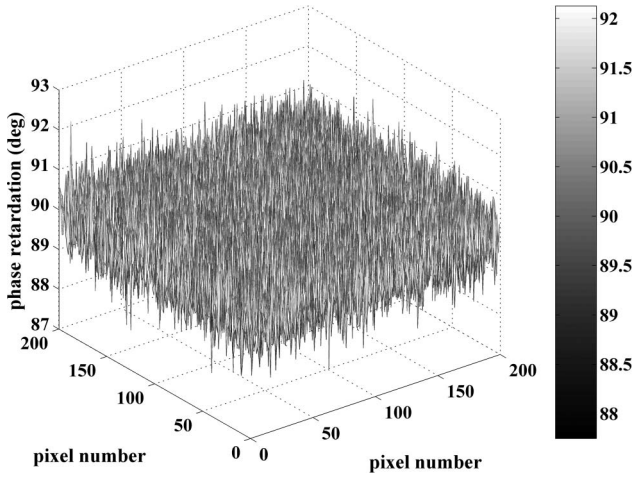

Fig. 7. Measured full-field phase retardation distribution of the quarter-wave-plate.

remains unchanged, and there is no characteristic phase. Its errors may be influenced by the sampling error $\Delta\phi_s = 0.036°$ and the polarization-mixing error $\Delta\phi_p = 0.03°$ [1]. Consequently, the total theoretical error is $\Delta\phi = \Delta\phi_s + \Delta\phi_p = 0.066°$. Hence, the operation of the whole process is simpler, faster, and more accurate than the previous method.

5. Conclusion

An improved technique for full-field absolute phase measurements in the heterodyne interferometer with an electro-optic modulator has been proposed in this paper. When an asymmetric triangle voltage signal is applied to drive the electro-optic modulator, the interference signals become two groups of periodic sinusoidal segments with different frequencies. These two groups of segments are fitted by the least-squares sine fitting algorithm, and their associated phases can be determined. By subtracting the initial phase of these two groups, the absolute phase can be obtained. This technique is applied to all pixels, and the full-field absolute phase measurements can be achieved. The validity of this method has been demonstrated.

This study was supported in part by the National Science Council of Taiwan (NSCT) under contract NSC95-2221-E009-236-MY3.

References

1. Y. L. Chen and D. C. Su, "Method for determining full-field absolute phases in the common-path heterodyne interferometer with an electro-optic modulator," Appl. Opt. **47**, 6518–6523 (2008).
2. N. A. Massie, R. D. Nelson, and S. Holly, "High-performance real-time heterodyne interferometry," Appl. Opt. **18**, 1797–1803 (1979).
3. R. Dandliker, R. Thalmann, and D. Prongue, "Two-wavelength laser interferometry using superheterodyne detection," Opt. Lett. **13**, 339–341 (1988).
4. E. Gelmini, U. Minoni, and F. Docchio, "Tunable, double-wavelength heterodyne detection interferometer for absolute-distance measurements," Opt. Lett. **19**, 213–215 (1994).
5. C. M. Feng, Y. C. Huang, J. G. Chang, M. Chang, and C. Chou, "A true sensitive optical heterodyne polarimeter for glucose concentration measurement," Opt. Commun. **141**, 314–321 (1997).
6. T. Tkaczyk and R. Jozwicki, "Full-field heterodyne interferometer for shape measurement: experimental characteristics of the system," Opt. Eng. **42**, 2391–2399 (2003).
7. M. C. Pitter, C. W. See, and M. G. Somekh, "Full-field heterodyne interference microscope with spatially incoherent illumination," Opt. Lett. **29**, 1200–1202 (2004).
8. P. Egan, M. J. Connely, F. Lakestani, and M. P. Whelan, "Random depth access full-field heterodyne low-coherence interferometry utilizing acousto-optic modulation and a complementary metal-oxide semiconductor camera," Opt. Lett. **31**, 912–914 (2006).
9. M. Akiba, K. P. Chan, and N. Tanno, "Full-field optical coherence tomography by two-dimensional heterodyne detection with a pair of CCD cameras," Opt. Lett. **28**, 816–818 (2003).
10. Y. L. Lo, H. W. Chih, C. Y. Yeh, and T. C. Yu, "Full-field heterodyne polariscope with an image signal processing method for principal axis and phase retardation measurements," Appl. Opt. **45**, 8006–8012 (2006).
11. IEEE, "Standard for terminology and test methods for analog to digital converters," IEEE Std 1241-2000, 25–29 (2001).